
Exploring through Random Curiosity with General Value Functions

Aditya Ramesh¹ Louis Kirsch¹ Sjoerd van Steenkiste^{2*} Jürgen Schmidhuber^{1,3,4}

¹The Swiss AI Lab (IDSIA), University of Lugano (USI) & SUPSI

²Google Research

³AI Initiative, King Abdullah University of Science and Technology (KAUST)

⁴NNAISENSE

{aditya, louis, juergen}@idsia.ch, svansteenkiste@google.com

Abstract

Efficient exploration in reinforcement learning is a challenging problem commonly addressed through *intrinsic* rewards. Recent prominent approaches are based on *state novelty* or variants of *artificial curiosity*. However, directly applying them to partially observable environments can be ineffective and lead to premature dissipation of intrinsic rewards. Here we propose random curiosity with general value functions (RC-GVF), a novel intrinsic reward function that draws upon connections between these distinct approaches. Instead of using only the current observation’s novelty or a curiosity bonus for failing to predict precise environment dynamics, RC-GVF derives intrinsic rewards through predicting temporally extended general value functions. We demonstrate that this improves exploration in a hard-exploration diabolical lock problem. Furthermore, RC-GVF significantly outperforms previous methods in the absence of ground-truth episodic counts in the partially observable MiniGrid environments. Panoramic observations on MiniGrid further boost RC-GVF’s performance such that it is competitive to baselines exploiting privileged information in form of episodic counts.

1 Introduction

How should an agent efficiently explore environments with high-dimensional state spaces and sparse rewards [70, 2]? An *extrinsic* reward-maximising agent will make little progress until it stumbles upon a rewarding sequence of actions. In the literature, this issue is commonly addressed by providing additional *intrinsic* reward to guide the agent’s exploratory behaviour [49, 12, 43].

One class of prominent approaches rely on *state novelty*, where an intrinsic reward in the form of a ‘novelty bonus’ is awarded based on how often a state has been visited [65, 6]. More recent works have extended these approaches to high dimensional state spaces where tabular counts are inapplicable [7, 41, 10]. Another class of approaches is based on *artificial curiosity*, where agents are rewarded in proportion to the prediction errors or information gains of a predictive world model [52, 60]. Curiosity-based techniques have also been scaled up to handle larger state spaces [22, 43].

Expecting an agent to have access to the complete environment state is unrealistic. In such *partially observable* settings [3, 26], observations may look alike in different states, and the benefit of approximate state novelty bonuses as intrinsic rewards is unclear. Consider the environment in Figure 1 where an agent is required to traverse a series of blue and white tiles, yet it is only able to observe the current tile it is standing on. The colours of the tiles alternate in a regular fashion until the end of the corridor, where there is a surprising sequence of consecutive blue tiles. Directly

*Part of this work was done while the author was a Postdoctoral researcher at IDSIA.

applying state novelty approaches may not be particularly meaningful in this case, as can be seen when using random network distillation (RND; [10]). In RND, the agent receives a novelty bonus based on the error of its predictions about the output of a fixed randomly initialised neural network applied to the current observation. As shown in the top panel of Figure 1, RND is unable to ascribe novelty when the state pattern changes later in the sequence and the intrinsic reward has vanished. Similarly, intrinsic rewards may also vanish prematurely for certain curiosity-based approaches when single-step dynamics are simple [42], while longer horizon predictions (as needed in the partially observable case) are susceptible to rapidly compounding errors during sequential rollouts [69].

In this paper, we explore a connection between state novelty and artificial curiosity to address these limitations. We propose *random curiosity with general value functions (RC-GVF)* as a novel approach to generating intrinsic rewards. It takes inspiration from exploration through temporally extended experiments that summarise long observation sequences [53]. Our approach uses random general value functions (GVFs) [67] to pose questions about the cumulative future value of observation-dependent features. Specifically, we train an ensemble of predictors to minimise the temporal difference (TD) errors of the general value functions and derive an intrinsic reward based on the TD-errors and disagreements in the long-term predictions. The effective horizon of the prediction task can be controlled via the discount factor, where a zero discount can be related to state novelty with random network distillation (RND) [10]. We hypothesise that predicting information from an temporally extended horizon improves exploration in POMDPs and guards against premature vanishing of intrinsic rewards due to the increase in difficulty of the auxiliary task. Indeed, in our toy experiment of Figure 1 it can be seen how RC-GVF manages to generate a spike of intrinsic reward at the end of the sequence.

We evaluate our approach on sparse-reward and partially observable RL problems. Our results on a hard exploration diabolical lock problem [36] and the Minigrid suite of environments [13] reveal the benefits of considering extended horizon predictions in comparison to approaches that rely on immediate partial observations to generate exploration bonuses. Furthermore, existing baselines in Minigrid are heavily reliant on privileged information about episodic state-visitation counts from the simulator, which is commonly used to scale the exploration bonus. We demonstrate that RC-GVF succeeds in many environments *without* the use of such episodic counts.

2 Preliminaries

Reinforcement learning in POMDPs We consider the scenario where an agent interacts with a Partially Observable Markov Decision Process (POMDP) with time steps $t \in \mathbb{N}$, with environment states $S_t \in \mathcal{S}$, observations $O_t \in \mathcal{O}$, actions $A_t \in \mathcal{A}$, extrinsic rewards $R_e : \mathcal{S} \rightarrow [0, 1]$, and policies that map histories of different lengths to distributions over actions $\pi : \mathcal{H} \rightarrow \Delta(\mathcal{A})$ where $H_t = O_{1:t} \in \mathcal{H}$ [26]. The agent only observes O_t at time step t , which may not fully describe the MDP state, and thus it becomes necessary to condition the agent on the history H_t .

The learning objective is to find the optimal policy π^* that maximizes the expected discounted return

$$J(\pi) = \mathbb{E}_\pi \left[\sum_{k=0}^{\infty} \gamma^k R_e(S_k) \right], \quad (1)$$

where $\gamma \in [0, 1)$ is the discount factor and the expectation is over stochastic components in the environment and the policy.

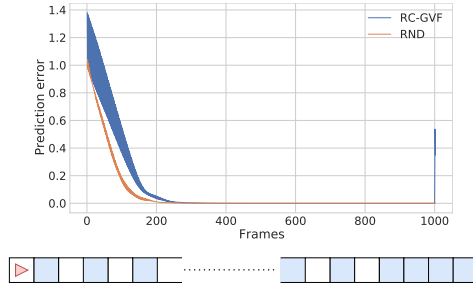


Figure 1: The alternating tile corridor environment. The agent (red triangle) observes the colour of the tile that it currently occupies (white or blue). The extrinsic reward is always zero. At each time-step (frame), the agent moves one tile forward, until it reaches the last tile. Unlike our approach (RC-GVF), RND does not generate an intrinsic reward when encountering the surprising last few tiles (step 1000).

Random Network Distillation In random network distillation (RND) [10] the agent receives a state novelty reward proportional to the error of making predictions $\hat{z}(o_t)$ where the targets are generated by a randomly initialized neural network $Z_\phi : \mathcal{O} \rightarrow \mathbb{R}^d$. The RND intrinsic reward for an observation is given by

$$R_i(o_t) = \|Z_\phi(o_t) - \hat{z}(o_t)\|_2. \quad (2)$$

RND-like error signals can be a simple way to obtain effective uncertainty estimates about targets at a given input, which could subsequently be used for exploration in RL or detecting out of distribution samples [14]. Beyond its simplicity, an appealing aspect of using RND is that it allows us to implicitly incorporate prior beliefs about useful rewards through the neural network architecture [38].

General Value Functions A general value function (GVF) [67] is defined by a policy π , a cumulant or pseudo-reward function $Z : \mathcal{O} \rightarrow \mathbb{R}$, and a discount factor $\gamma_z \in [0, 1)$. It can be expressed as

$$v_{\pi,z}(o) = \mathbb{E}_\pi \left[\sum_{k=0}^{\infty} \gamma_z^k Z(O_{t+k}) | O_t = o \right]. \quad (3)$$

General value functions extend the concept of predicting expected cumulative values to arbitrary signals beyond the reward. They can be viewed as ‘answering’ questions about cumulative quantities of interest under a particular policy π and discount factor γ_z . Predictions from GVFs have previously been used as features for state representation [47] or to specify auxiliary tasks that assist in shaping representations for the main task [24, 73].

3 Random Curiosity with General Value Functions

In the spirit of artificial curiosity [53], we are interested in predicting long-term outcomes in the environment under a particular policy as a means for exploration. Our approach, *RC-GVF*, rewards an agent for taking actions that lead to higher uncertainty about the future. However, instead of predicting the entire sequence of future states, we consider a set of random numeric questions about the environment and capture uncertainty about their outcome using general value functions (GVFs).

3.1 General value functions to predict the future

The central piece of RC-GVF is the prediction of temporally extended outcomes in the environment. This is different from only predicting a feature of the current state (as in state novelty exploration [65]) or dynamics models that predict the entire (sequence of) next observation(s) (as in early versions of artificial curiosity [52]). At time step t , the current observation o_t is mapped to a collection of pseudo-rewards $z_{t+1} \in \mathbb{R}^d$ which together with the policy and discount factor define a question that can be asked about the future: “what is the expected discounted cumulative sum of these pseudo-rewards under a given policy?”. The answer to this question (i.e. the prediction target) is based on outcomes in the environment, as in Equation 3. In this paper, we investigate whether a set of random pseudo rewards are sufficient to drive exploration in this way.

Previously it was found that random features extracted by a neural network are often sufficient to capture useful properties of the input [45]. Similarly, neural network architectures can be used to express prior knowledge about useful features [71, 14]. To this end, we generate pseudo-rewards from a fixed and randomly initialised neural network $Z_\phi : \mathcal{O} \rightarrow \mathbb{R}^d$ with parameters ϕ that maps observations to pseudo-rewards. This choice also bypasses the difficult problem of discovering meaningful general value functions [73].

Training the GVF predictors Our exploration mechanism is to reward the agent for taking actions that generate previously unknown outcomes. To facilitate this, we train a separate (recurrent) neural network—which we call the *predictor*—to predict these values. Concretely, a predictor $\hat{v}_{\pi,z} : \mathcal{H} \rightarrow \mathbb{R}^d$ maps histories (of observations, actions, and pseudo rewards) to pseudo-values.

The predictor is trained on-policy, implying that the GVFs are evaluated under the current policy. One motivating factor for this choice is that it couples the prediction task to the current policy, thus creating an incentive to vary behaviour for additional exploration [18].

We use the (truncated) λ -return as the target for the predictor, which can be recursively expressed as

$$G_t^z(\lambda_z) = Z_{t+1} + \gamma_z(1 - \lambda_z)\hat{v}_{\pi,z}(H_{t+1}) + \gamma_z\lambda_z G_{t+1}^z(\lambda_z). \quad (4)$$

Here, $\lambda_z \in [0, 1]$ is the usual parameter that allows balancing the bias-variance trade off by interpolating between TD(0) and Monte Carlo estimates of the pseudo-return [64]. The predictor is trained to minimise the mean squared TD-error with the λ -return target. For convenience in notation, we will denote $G_t^z(\lambda_z)$ as G_t^z , despite its dependence on λ_z .

3.2 Disagreement and prediction error as intrinsic reward

To generate an intrinsic reward, a straightforward choice could be to consider the error between the temporal difference target (from Equation 4) and the predictor’s output at the current observation:

$$L_{\text{TD}}(h_t) = [G_t^z - \hat{v}_{\pi,z}(h_t)]^2. \quad (5)$$

However, the presence of *aleatoric* uncertainty is a problem that arises as a consequence of extending the horizon of the predictive task. From an exploration perspective, the agent should focus on the reducible *epistemic* uncertainty, and not the irreducible aleatoric uncertainty [15, 23]. Directly minimising Equation 5 with the predictor would ignore the inherent variance in the TD-target (due to stochasticity in the policy and environment), and thus using the prediction error of the GVF target as an intrinsic reward does not distinguish between aleatoric and epistemic uncertainty.

Another way to recognize this is by decomposing the expected prediction error as described by Jain et al. [25]. The expected loss of a predictor $\hat{f}(\cdot)$ at an input o , $\mathbb{E}[L(t, \hat{f}(o))]$, can be split into epistemic (E) and aleatoric (A) components: $\int L(t, \hat{f}(o))dP(t|o) = E(\hat{f}, o) + A(o)$, where $P(t|o)$ is the conditional distribution over targets for input o and $L(t, \cdot)$ is a chosen loss function. The aleatoric uncertainty at input o , $A(o)$, is defined as the expected prediction error of a Bayes optimal predictor function. $E(\hat{f}, o)$ denotes the epistemic uncertainty of a predictor at o .

To overcome this issue with aleatoric uncertainty in RC-GVF, we propose to train an *ensemble* of predictors and utilise the variance across their predictions as a multiplicative factor on the prediction error. Concretely, we train K predictors $\hat{v}_{\pi,z}^k, k \in \{1, 2 \dots K\}$. The prediction target for each member of the ensemble is the same λ -pseudo-return (Equation 4) by using bootstrapped values from that member’s predictions. Using the ensemble of predictors, the intrinsic reward is given by

$$R_i(o_t) = \sum_{j=1}^d \left(\mathbb{E}[L_{\text{TD}}^k(h_t)] \odot \mathbb{V}[\hat{v}_{\pi,z_j}^k(h_t)] \right)_j \quad (6)$$

$$= \sum_{j=1}^d \left[\frac{1}{K} \sum_{k=1}^K \left(G_t^{z_j} - \hat{v}_{\pi,z_j}^k(h_t) \right)^2 \right] \cdot \left[\frac{1}{K-1} \sum_{k=1}^K \left(\bar{v}_{\pi,z_j}(h_t) - \hat{v}_{\pi,z_j}^k(h_t) \right)^2 \right], \quad (7)$$

where \odot corresponds to element-wise multiplication. In this formulation, even when prediction error remains, the exploration bonus will vanish as the predictors converge to the same expectation.

3.3 Effective horizon and relation to random network distillation

The effective horizon over which predictions are considered depends on the choice of the discount factor γ_z . It can be shown that for a horizon $H_{\gamma_z, \varepsilon} \in \mathbb{R}$ satisfying

$$H_{\gamma_z, \varepsilon} \geq \frac{\log\left(\frac{1}{\varepsilon(1-\gamma_z)}\right)}{\log\left(\frac{1}{\gamma_z}\right)}, \quad (8)$$

the discounted sum of (pseudo) rewards beyond this horizon is bounded by ε [28, 30].

From Equation 4 we can see that for the special case of $\gamma_z = 0$ and any choice of λ_z , we have $G_t^z = Z_{t+1} = Z_\phi(o_t)$. Note that in this case the TD-error between prediction and target is equivalent to the intrinsic reward provided by random network distillation (RND; Equation 2). Since the prediction targets are now deterministic, there is no problem with aleatoric uncertainty, and a single predictor suffices (as opposed to an ensemble).

4 Related work

Exploration In tabular RL, explicit *counts* for states or state-action pairs can be maintained to enable exploration and achieve efficient learning [61, 4]. Count-based bonuses have been scaled to larger state spaces through the use of density models, which provide pseudo-counts [7, 41]. State novelty bonuses are similarly inspired heuristics that provide a bonus based on estimated novelty of the visited state [10].

Perhaps the simplest way of implementing exploration through ‘*curiosity*’ is to reward the policy for encountering transitions to states that surprise a learning predictor [52]. This is suitable for deterministic environments but it suffers from the ‘noisy TV problem’ in stochastic environments [56, 9]. To overcome this limitation, intrinsic rewards have been defined by *learning progress* (the first derivative of the prediction error) [51], *information gain* [60, 22], or *compression progress* [55]. Also compare such bonuses to pseudo-counts [7]. Alternatively, it is possible to mitigate sensitivity to noise by measuring prediction errors in a latent space [53, 43].

Our method is different from state count and novelty approaches in that it models temporally extended values beyond the current observation. It includes a state-novelty measure, RND [10], as a special case when the GVF discount factors are zero. Unlike most artificial curiosity approaches, RC-GVF does not model the entire environment dynamics, in line with the idea of conducting temporally extended experiments whose outcomes are abstract summaries (represented in latent variables) of long observation sequences [54]. We mitigate sensitivity to aleatoric uncertainty by measuring the disagreement of an *ensemble* of predictors, inspired by prior work (for single-step prediction models) [59, 44]. Ensembles for exploration have also been explored in the context of posterior sampling [62]. Bootstrapped-DQN [38] uses an ensemble of Q-value functions for a model-free interpretation of posterior sampling [39]. Unlike in our approach, these value functions are restricted to the original task rewards, and can not capture arbitrary pseudo-rewards. Recent works suggest incorporating model-based planning to directly optimise for long-term novelty [63, 58, 31]. Our intrinsic reward—which is generated by considering multiple future steps—could motivate approaches for optimising long-term novelty without explicit rollout-based planning.

General Value Functions Sutton et al. [67] proposed general value functions (GVFs) as an approach to represent predictive knowledge about the world. Closely related is the vector-valued adaptive critic [50] which predicts and controls cumulative values of special input vectors. Several works have studied the impact of using auxiliary value functions to improve representation learning in RL [24, 8, 35]. Further, it was previously found that GVFs of randomly generated pseudo-rewards can also be useful for shaping and learning representations [34, 78] (see also related work on forecasts [47], TD-networks [66], and predictive state representations [32]). This can be viewed as ‘answering’ questions about cumulative quantities of interest under a particular policy π and discount factor γ_z . In our implementation, the predictor is an entirely separate network and thus GVF prediction can not be used to improve the agent’s internal representation. Instead, we use the GVF prediction to derive a useful signal to guide exploration.

The discovery/selection of useful GVF ‘questions’ is an open problem [48]. Existing approaches learn questions related to optimizing performance on the main task [73, 27]. However, such an approach might not be suitable for sparse-reward environments. In our approach, we side-step the GVF discovery problem through the use of randomly generated pseudo-rewards and on-policy predictions.

5 Experiments

In this section we present an empirical evaluation of RC-GVF.² First, we consider a hard exploration diabolical lock problem from the literature [36] and demonstrate the benefits of predicting beyond the immediate observation. We then proceed to experiments with the standard Minigrid suite of partially observable and procedurally generated environments, demonstrating how RC-GVF is able to outperform several strong baselines [18, 77].

²Code is available at <https://github.com/Aditya-Ramesh-10/exploring-through-rcgvf>.

5.1 Diabolical locks

The diabolical lock problem [36] is considered a difficult environment for exploration due to noisy high-dimensional observations, stochastic dynamics and misleading rewards that deter the agent from finding the sparse optimal reward at the end of the lock. In the literature, RND is often shown to fail on these types of environments due to only considering the immediate future [36]. Due to RC-GVF’s policy-conditioned predictions of future quantities, this task is instructive to demonstrate the qualitative advantages of our method and how this results in markedly different performance.

Environment details The environment consists of states organised in 3 rows $\{a, b, c\}$ and H columns from $\{1, 2, \dots, H\}$ (see Figure 6 in Appendix A.1). In each episode, the agent is initialised in one of two possible starting states, either at a_1 or b_1 . At each state the agent has L available actions, only one of which is ‘good’ and transitions to a ‘good’ state in the next column with equal probability. Taking the good action gives a negative (anti-shaped) reward of

$-1/H$, except at the end of the lock (states a_H or b_H), where the sparse optimal reward of 10 is received. The remaining $L - 1$ actions at any state are ‘bad’, causing a deterministic transition to the ‘dead’ row c at the next column (zero reward). All actions from a dead state lead to the dead state in the next row, and hence the optimal policy is to take the respective good actions in each state. The good action at each state is assigned randomly as part of the MDP specification. The agent never observes the state directly and only has access to a high-dimensional noisy observation (details in Appendix A.1).

In our experiment, we consider a problem with horizon $H = 100$, $L = 10$, and observation noise $\sigma_o = 0.1$. As discussed by Misra et al. [36], this exploration problem is hard because the probability of reaching the optimal reward through a uniformly random policy is L^{-H} (10^{-100} in our instance). Further, the stochastic transitions from good states prevent a solution that relies on memorising a state-independent successful sequence of H actions independent of the state.

Implementation We use Proximal Policy Optimization (PPO) [57] in an actor-critic framework as the base agent and use 128 pseudo-rewards for RND and RC-GVF. For RC-GVF we set $\gamma_z = 0.6$ and use two prediction heads in the ensemble. The agent is trained to maximize the expected sum of a weighted combination of intrinsic and extrinsic rewards. Further details are in Appendix A.1.

Results Table 1 compares RND to RC-GVF in this environment. It can be seen how RC-GVF succeeds in completing the lock on all runs, while the best run of RND only reaches 60% of the lock (and does not complete it). Indeed, once the agent takes an incorrect action and ‘falls’ into the bottom row, the future consequences (and thus, the GVFs) become highly predictable. By staying alive, the agent will encounter new observations and unpredictable transitions which appear interesting. Further experiments with additional baselines are presented in Appendix D. This result is illustrative of RC-GVFs exploration capabilities as we will see next.

5.2 MiniGrid

We evaluate RC-GVF on procedurally generated environments from MiniGrid [13], which is a standard benchmark in the deep reinforcement learning literature for exploration [46, 11, 18, 77, 76, 42]. Exploration in these environments is challenging due to partial observability, extremely sparse rewards, and the procedural generation of mazes and objects.

Environment Details Broadly speaking, we will consider three classes of environments organised according to several difficulty levels. First, we study *MultiRoom-N7-S8* and *MultiRoom-N12-S10*, which are navigation tasks in a maze with seven and twelve rooms respectively. Next, we consider two levels of difficulty in *KeyCorridor-S4R3* and *KeyCorridor-S5R3*. Here, the agent needs to pick up a ball behind a locked door. Finally, we examine the *ObstructedMaze* set of environments where the agent has a similar task of picking up a ball behind a locked door, but keys are hidden in boxes (*ObstructedMaze-2Dlh*), and doors can be obstructed (*ObstructedMaze-2Dlhb*). The observations

Table 1: Mean over 10 seeds and (min, max) of the farthest column reached (of $H = 100$) at different points on the diabolical lock problem.

Frames	5M	10M	20M
RC-GVF	61 (47, 81)	94 (83, 100)	100 (100, 100)
RND	28 (21, 41)	37 (27, 47)	46 (33, 58)

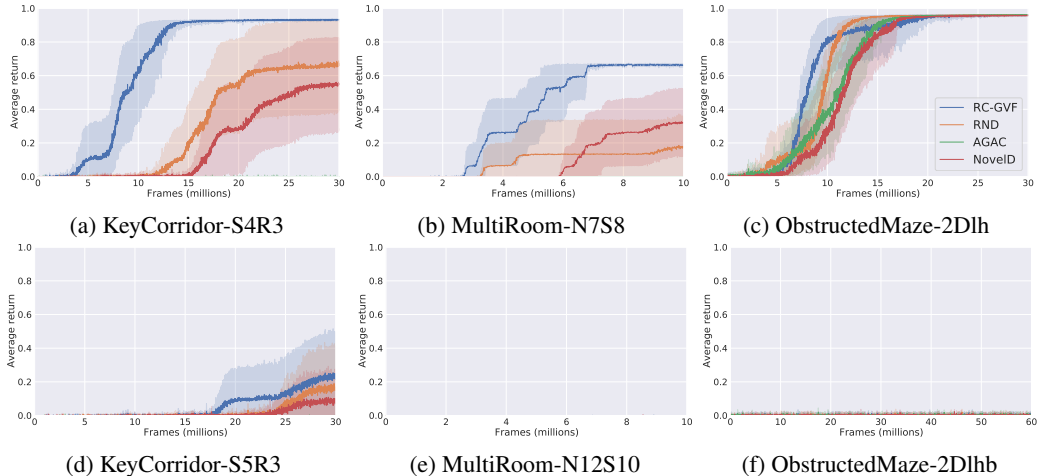


Figure 2: Average return of RC-GVF, RND and other baselines on the selected MiniGrid environments (without ground-truth episodic counts for baselines). RC-GVF outperforms baselines in the absence of episodic counts. Some environments prove challenging for all approaches in this setting.

corresponds to an egocentric view of the cells in the front of the agent. Further details of the MiniGrid environments are available in Appendix A.2.

Implementation We compare RC-GVF to RND [10], AGAC [18], and NovelD [77]. We use Proximal Policy Optimization (PPO) [57] as our base agent for all approaches. The agent is trained to maximize the expected sum of a weighted combination of intrinsic and extrinsic rewards. At each time step t , the agent receives a reward $R_t = R_e(s_t) + \beta R_i(o_t)$, where $\beta \in \mathbb{R}_+$ balances the contribution of the extrinsic $R_e(s_t)$ and intrinsic $R_i(o_t)$ rewards. For RC-GVF we set $\gamma_z = 0.6$, use two prediction heads in the ensemble of predictors and use 128 pseudo-rewards (same as for RND). Other important hyper-parameters, such as the intrinsic reward coefficient (β), entropy coefficient, and learning rate of the predictor are obtained via an extensive hyper-parameter search for all baselines (see Appendices C.2 and C.3 for details, including on our implementation of baselines.).

We present results averaged over 10 independent runs for each approach in every figure (solid line). Unless mentioned otherwise, the shading indicates 95% bootstrapped confidence intervals.

5.2.1 Egocentric observations

We will first consider the usual setting where the agent receives access to the egocentric observations from the environment. Importantly, we do not provide agents with access to privileged information about the environment in the form of so-called ‘episodic counts’. This is different from several recent approaches that have been applied to MiniGrid, which incorporate these values as part of their intrinsic reward [46, 18, 77].

The use of episodic counts obtained through the simulator is problematic for solving exploration problems in a partially observable setting, since it tells the agent precisely how frequently it has been in each state. Indeed, the use of episodic counts *alone* can be sufficient for exploration in MiniGrid (Figure 7 in Appendix E.1). Meanwhile, there exists no good method for obtaining episodic counts in the absence of a simulator, as it is difficult to accurately estimate pseudo-counts from partial observations (eg. as in Figure 1). Details about the exact usage of episodic counts by baselines in their intrinsic reward formulation are provided in Appendix C.2.

In Figure 2 we compare RC-GVF, RND, AGAC, and NovelD in the absence of episodic counts, while using egocentric observations. It can be seen that RC-GVF explores faster and succeeds more often than RND and the other baselines in the KeyCorridor-S4R3 environment and MultiRoom-N7-S8 environment. In comparison to RND and NovelD that utilise prediction errors in immediate random embeddings, it appears that RC-GVF benefits from extended horizon predictions of random pseudo-rewards. Meanwhile, AGAC only succeeds in ObstructedMaze-2Dlh, where all baselines perform similarly well. Finally, we observe that all approaches struggle with the most difficult level of considered environments (KeyCorridor-S5R3, MultiRoom-N12-S10 and ObstructedMaze-2Dlhb).

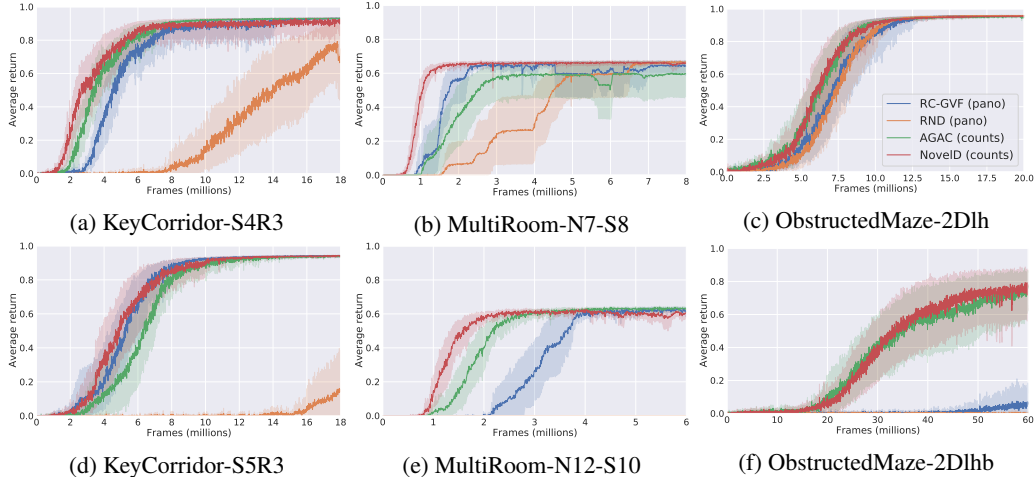


Figure 3: Average return of RC-GVF and RND with panoramic observations. The performance of baselines (AGAC and NovelD) improves significantly with the inclusion of the episodic count component while RC-GVF (using panoramic observations) achieves similar performance without.

5.2.2 Panoramic observations

We now demonstrate how using episodic counts from the simulator is crucial to the success of the baselines. In Figure 3 it can be seen how AGAC and NovelD improve with episodic counts, and also solve the more difficult problems (KeyCorridor-S5R3, MultiRoom-N12-S10 and ObstructedMaze-2Dlh).

Panoramic observations In order to increase performance of RC-GVF further, without introducing episodic counts, we investigate the use of augmented panoramic views as previously explored by Parisi et al. [42]³. In the MiniGrid environments, the observation changes almost in its entirety when the agent changes the direction it faces. In contrast, moving to the next cell leads to fewer sudden changes in the observation.

The lack of gradual changes of egocentric observations through rotations is a consequence of having four discrete angles for orientation ($0^\circ, 90^\circ, 180^\circ, 270^\circ$), which may be an unrealistic depiction of how rotations affect observations for agents situated in the real world. As a consequence, prediction errors are dominated by predictions of the outcomes of turning (rather than other actions). To address this, prior work proposed to make the agent’s observations invariant to rotation by augmenting the observation with all directional observations [42]. In effect, this assumes that the agent rotates 360° after moving to a cell, or alternatively that it is equipped with additional sensors on its sides and back. Similar to Parisi et al. [42], we will consider panoramic views only for generating intrinsic rewards, and egocentric observations for the base PPO agent.

In Figure 3, we demonstrate how RC-GVF with panoramic views and without privileged information about the underlying state of the MDP can solve harder problems and is competitive with the baselines that use episodic counts in five out of the six settings. We see that RC-GVF with panoramic observations comfortably succeeds in the KeyCorridor-S5R3 and MultiRoom-N12-S10 environments where it was previously unsuccessful. RC-GVF did not succeed in solving the harder ObstructedMaze-2Dlh within the given frames despite the inclusion of panoramic views. Figure 3 shows that the use of panoramic views does not make the exploration problem trivial; RND also uses panoramic views (but no episodic counts). It improves with panoramic views on KeyCorridor-S4R3 and MultiRoom-N7S8 but struggles with the harder instances.

5.3 Analysis

Changing the temporal prediction horizon We study the effect of changing the temporal prediction horizon by evaluating RC-GVF with different discount factors. Recall from Equation 8

³We verified in a preliminary experiment that incorporating episodic counts for RC-GVF similarly improves performance (see Figure 8 in Appendix E.2). However, since we believe that this constitutes privileged information that is not readily accessible outside of a simulator, we will not explore this direction further.

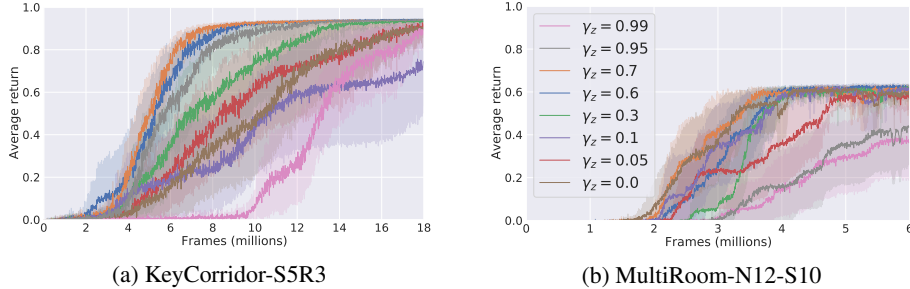


Figure 4: Analysis reveals that: (a) larger discount factors (except 0.99) are useful in KeyCorridor-S5R3 (b) low and intermediate discount factors perform well in MultiRoom-N12-S10.

how the discount factor can be mapped to the prediction horizon, which lets us estimate a lower bound on the horizon of about 11 time steps for $\gamma_z = 0.6$ with $\epsilon = 0.01$. In Figure 4 it can be seen how a larger prediction horizon is desirable for KeyCorridorS5R3. Among the higher discount factors, 0.95 is a good choice for this environment, but not 0.99. Compared to our default value of $\gamma_z = 0.6$, a short horizon using 0.3 reduces performance further, while discount factors closest to 0 yield worse performance. In contrast, for MultiRoom-N12-S10, we find that low and intermediate values of γ_z perform well. The high GVF discount factors of 0.99 and 0.95 perform worse. Comparing $\gamma_z = 0$ to RND shows how the use of recurrent networks and the variance term derived from the ensemble of predictors contributes most to the performance of RC-GVF in this domain.

Ablation To better understand which of these components are contributing most to the success of RC-GVF, we consider the following additional ablations: (1) RC-GVF ($\gamma_z = 0$) without the variance term in Equation 6, and (2) RC-GVF ($\gamma_z = 0$) without the recurrent predictor. Figure 5a compares these variations to RC-GVF ($\gamma_z = 0$), RC-GVF ($\gamma_z = 0.6$), and RND. It can be seen that the inclusion of the history-conditioned recurrent predictor and the variance term individually contribute to the improved performance of RC-GVF.

Using the history conditioned recurrent predictor sharply improves the performance of RC-GVF with $\gamma_z = 0$. We hypothesise that this effect arises from the previous pseudo-rewards available to the predictor, which might enable better predictions on input observations it was not explicitly trained on (which is often the case in procedurally generated environments). In support of this hypothesis, we observed that using a recurrent predictor with solely observations as inputs does not produce such an improvement (Figure 9 in Appendix E.3).

In Figure 5b, we present ablations for $\gamma_z = 0.6$. We consider RC-GVF without the variance term in Equation 6, and without the recurrent predictor. Removing either the disagreement term or the recurrent predictor worsens the performance of RC-GVF with $\gamma_z = 0.6$. Interestingly, unlike as was observed for $\gamma_z = 0$, here we find that RC-GVF with only disagreement (no recurrent predictor) performs better than RC-GVF with only recurrent predictor (no disagreement). This further emphasises the importance of handling the aleatoric uncertainty for non-zero GVF discounts.

Increasing the ensemble size We conduct experiments with larger ensemble sizes in two MiniGrid environments. We obtain comparable results for ensemble sizes of 2, 4, 6 and 8 predictors in Figure 10 in Appendix E.4, indicating that two member ensembles usually suffice for these problems.

6 Limitations and Societal Impact

Limitations The incorporation of the current policy into the prediction task of GVF prediction can have benefits with regards to behavioural exploration. However, it may also encourage over-exploration due to the same state appearing ‘interesting’ under different policies. Possible mitigation strategies include off-policy variants or explicitly policy-conditioned (general) value functions [17, 20].

In some situations it may be difficult to ascertain what is a good choice of the GVF discount factor γ_z , which effectively determines the prediction horizon length, and can be influenced by optimisation effects under function approximation [72]. The best choice may be problem-dependent and could

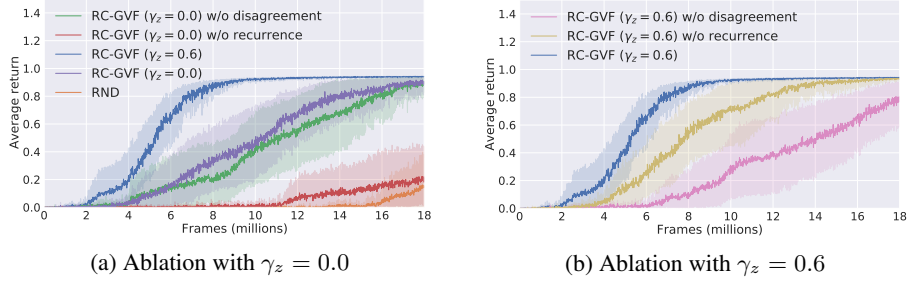


Figure 5: Ablation of RC-GVF components in the KeyCorridor-S5R3 environment (a) the variance term, recurrent predictor and discount factor contribute most to the performance of RC-GVF (b) the variance term appears to be more important in the case of $\gamma_z = 0.6$.

further benefit from dynamic adjustment during learning [5, 37]. Nonetheless, our results in Figures 2 and 3 indicate that a default of $\gamma_z = 0.6$ works well in many of the considered settings.

Several other intrinsic reward formulations using RC-GVF are possible (eg. based on information/prediction gain, learning progress, or only the disagreement term), which we did not investigate. Our specific formulation in Equation 6 was motivated by the prediction error in RND, which does not separate the aleatoric uncertainty when $\gamma_z > 0$. Starting with the prediction error term also allowed us to closely study the connection between RND and RC-GVF.

A general limitation of curiosity-based exploration for task-specific RL is that more information is gathered than is necessary to solve the given task [40, 33]. Indeed, the space of potential GVFs is enormous. In the case of RC-GVF one could aim at focusing it by integrating task-specific information [68] or by considering predictions using a smaller set of policies that adequately cover the state space [1].

Societal impact This paper does not focus on real-world applications of exploration in RL and thus does not have a direct societal impact. In applications, advanced exploration methods may lead to unexpected policy behaviour, which could be mitigated by incorporating safety constraints [19].

7 Conclusion

We introduced *random curiosity with general value functions (RC-GVF)*, an exploration method that intrinsically rewards a reinforcement learning agent based on errors and uncertainty in predicting random transformations of observation sequences generated through the agent’s actions. Unlike state-novelty approaches, ours takes into account multi-step future behaviours of policy and environment. Unlike commonly used artificial curiosity approaches, RC-GVF does not rely on model rollouts and does not need to predict all details of future observations.

On the diabolical lock problem [36] and the MiniGrid environments [13] we demonstrate that predicting abstract quantities of extended time intervals can improve exploration in POMDPs. Compared to recent methods such as AGAC [18] and NovelD [77] that rely on privileged episodic state-visitation counts in MiniGrid, our RC-GVF achieves competitive results even when using only panoramic observations. Importantly, in the natural setting where episodic counts are not available, RC-GVF significantly outperforms all baseline methods.

Our approach can be generalized by moving beyond random pseudo-rewards, considering general value functions under a set of different policies [1], and introducing time or state-dependent discounting. This offers exciting avenues for future research.

Acknowledgments and Disclosure of Funding

We would like to thank Kenny Young, Francesco Faccio, Anand Gopalakrishnan, and Dylan Ashley for valuable comments. This research was supported by the ERC Advanced Grant (742870), the Swiss National Science Foundation grant (200021_192356), and by the Swiss National Supercomputing Centre (CSCS projects s1090 and s1127).

References

- [1] A. Agarwal, M. Henaff, S. Kakade, and W. Sun. Pc-pg: Policy cover directed exploration for provable policy gradient learning. *Advances in Neural Information Processing Systems*, 33: 13399–13412, 2020.
- [2] S. Amin, M. Gomrokchi, H. Satija, H. van Hoof, and D. Precup. A survey of exploration methods in reinforcement learning. *arXiv preprint arXiv:2109.00157*, 2021.
- [3] K. J. Åström. Optimal control of markov processes with incomplete state information. *Journal of mathematical analysis and applications*, 10(1):174–205, 1965.
- [4] P. Auer, T. Jaksch, and R. Ortner. Near-optimal regret bounds for reinforcement learning. *Advances in neural information processing systems*, 21, 2008.
- [5] A. P. Badia, B. Piot, S. Kapturowski, P. Sprechmann, A. Vitvitskyi, Z. D. Guo, and C. Blundell. Agent57: Outperforming the atari human benchmark. In *International Conference on Machine Learning*, pages 507–517. PMLR, 2020.
- [6] A. G. Barto and S. P. Singh. On the computational economics of reinforcement learning. In *Connectionist Models*, pages 35–44. Elsevier, 1991.
- [7] M. Bellemare, S. Srinivasan, G. Ostrovski, T. Schaul, D. Saxton, and R. Munos. Unifying count-based exploration and intrinsic motivation. *Advances in neural information processing systems*, 29:1471–1479, 2016.
- [8] M. Bellemare, W. Dabney, R. Dadashi, A. Ali Taiga, P. S. Castro, N. Le Roux, D. Schuurmans, T. Lattimore, and C. Lyle. A geometric perspective on optimal representations for reinforcement learning. *Advances in neural information processing systems*, 32, 2019.
- [9] Y. Burda, H. Edwards, D. Pathak, A. J. Storkey, T. Darrell, and A. A. Efros. Large-scale study of curiosity-driven learning. In *7th International Conference on Learning Representations*, 2019.
- [10] Y. Burda, H. Edwards, A. J. Storkey, and O. Klimov. Exploration by random network distillation. In *7th International Conference on Learning Representations*, 2019.
- [11] A. Campero, R. Raileanu, H. Küttler, J. B. Tenenbaum, T. Rocktäschel, and E. Grefenstette. Learning with amigo: Adversarially motivated intrinsic goals. *arXiv preprint arXiv:2006.12122*, 2020.
- [12] N. Chentanez, A. Barto, and S. Singh. Intrinsically motivated reinforcement learning. *Advances in neural information processing systems*, 17, 2004.
- [13] M. Chevalier-Boisvert, L. Willems, and S. Pal. Minimalistic gridworld environment for openai gym. <https://github.com/maximecb/gym-minigrid>, 2018.
- [14] K. Ciosek, V. Fortuin, R. Tomioka, K. Hofmann, and R. E. Turner. Conservative uncertainty estimation by fitting prior networks. In *8th International Conference on Learning Representations, ICLR*, 2020.
- [15] A. Der Kiureghian and O. Ditlevsen. Aleatory or epistemic? does it matter? *Structural safety*, 31(2):105–112, 2009.
- [16] L. Espeholt, H. Soyer, R. Munos, K. Simonyan, V. Mnih, T. Ward, Y. Doron, V. Firoiu, T. Harley, I. Dunning, et al. Impala: Scalable distributed deep-rl with importance weighted actor-learner architectures. In *International Conference on Machine Learning*, pages 1407–1416. PMLR, 2018.
- [17] F. Faccio, L. Kirsch, and J. Schmidhuber. Parameter-based value functions. In *9th International Conference on Learning Representations*, 2021.
- [18] Y. Flet-Berliac, J. Ferret, O. Pietquin, P. Preux, and M. Geist. Adversarially guided actor-critic. In *9th International Conference on Learning Representations*, 2021.

- [19] J. Garcia and F. Fernández. A comprehensive survey on safe reinforcement learning. *Journal of Machine Learning Research*, 16(1):1437–1480, 2015.
- [20] J. Harb, T. Schaul, D. Precup, and P.-L. Bacon. Policy evaluation networks. *arXiv preprint arXiv:2002.11833*, 2020.
- [21] S. Hochreiter and J. Schmidhuber. Long short-term memory. *Neural computation*, 9(8): 1735–1780, 1997.
- [22] R. Houthoofd, X. Chen, Y. Duan, J. Schulman, F. De Turck, and P. Abbeel. Vime: Variational information maximizing exploration. *Advances in Neural Information Processing Systems*, 29: 1109–1117, 2016.
- [23] E. Hüllermeier and W. Waegeman. Aleatoric and epistemic uncertainty in machine learning: An introduction to concepts and methods. *Machine Learning*, 110(3):457–506, 2021.
- [24] M. Jaderberg, V. Mnih, W. M. Czarnecki, T. Schaul, J. Z. Leibo, D. Silver, and K. Kavukcuoglu. Reinforcement learning with unsupervised auxiliary tasks. *arXiv preprint arXiv:1611.05397*, 2016.
- [25] M. Jain, S. Lahlou, H. Nekoei, V. Butoi, P. Bertin, J. Rector-Brooks, M. Korablyov, and Y. Bengio. Deup: Direct epistemic uncertainty prediction. *arXiv preprint arXiv:2102.08501*, 2021.
- [26] L. P. Kaelbling, M. L. Littman, and A. R. Cassandra. Planning and acting in partially observable stochastic domains. *Artificial intelligence*, 101(1-2):99–134, 1998.
- [27] A. Kearney, A. Koop, J. Günther, and P. M. Pilarski. Finding useful predictions by meta-gradient descent to improve decision-making. *arXiv preprint arXiv:2111.11212*, 2021.
- [28] M. Kearns, Y. Mansour, and A. Y. Ng. A sparse sampling algorithm for near-optimal planning in large markov decision processes. *Machine learning*, 49(2):193–208, 2002.
- [29] D. P. Kingma and J. Ba. Adam: A method for stochastic optimization. In *3rd International Conference on Learning Representations*, 2015.
- [30] L. Kocsis and C. Szepesvári. Bandit based monte-carlo planning. In *European conference on machine learning*, pages 282–293. Springer, 2006.
- [31] N. Lambert, M. Wulfmeier, W. Whitney, A. Byravan, M. Bloesch, V. Dasagi, T. Hertweck, and M. Riedmiller. The challenges of exploration for offline reinforcement learning. *arXiv preprint arXiv:2201.11861*, 2022.
- [32] M. Littman and R. S. Sutton. Predictive representations of state. *Advances in neural information processing systems*, 14, 2001.
- [33] X. Lu, B. Van Roy, V. Dwaracherla, M. Ibrahimi, I. Osband, and Z. Wen. Reinforcement learning, bit by bit. *arXiv preprint arXiv:2103.04047*, 2021.
- [34] C. Lyle, M. Rowland, G. Ostrovski, and W. Dabney. On the effect of auxiliary tasks on representation dynamics. In *International Conference on Artificial Intelligence and Statistics*, pages 1–9. PMLR, 2021.
- [35] M. McLeod, C. Lo, M. Schlegel, A. Jacobsen, R. Kumaraswamy, M. White, and A. White. Continual auxiliary task learning. *Advances in Neural Information Processing Systems*, 34: 12549–12562, 2021.
- [36] D. Misra, M. Henaff, A. Krishnamurthy, and J. Langford. Kinematic state abstraction and provably efficient rich-observation reinforcement learning. In *International conference on machine learning*, pages 6961–6971. PMLR, 2020.
- [37] T. Moskovitz, J. Parker-Holder, A. Pacchiano, M. Arbel, and M. Jordan. Tactical optimism and pessimism for deep reinforcement learning. *Advances in Neural Information Processing Systems*, 34, 2021.

- [38] I. Osband, C. Blundell, A. Pritzel, and B. Van Roy. Deep exploration via bootstrapped dqn. *Advances in neural information processing systems*, 29, 2016.
- [39] I. Osband, B. Van Roy, and Z. Wen. Generalization and exploration via randomized value functions. In *International Conference on Machine Learning*, pages 2377–2386. PMLR, 2016.
- [40] I. Osband, J. Aslanides, and A. Cassirer. Randomized prior functions for deep reinforcement learning. *Advances in Neural Information Processing Systems*, 31, 2018.
- [41] G. Ostrovski, M. G. Bellemare, A. Oord, and R. Munos. Count-based exploration with neural density models. In *International conference on machine learning*, pages 2721–2730. PMLR, 2017.
- [42] S. Parisi, V. Dean, D. Pathak, and A. Gupta. Interesting object, curious agent: Learning task-agnostic exploration. *Advances in Neural Information Processing Systems*, 34, 2021.
- [43] D. Pathak, P. Agrawal, A. A. Efros, and T. Darrell. Curiosity-driven exploration by self-supervised prediction. In *International conference on machine learning*, pages 2778–2787. PMLR, 2017.
- [44] D. Pathak, D. Gandhi, and A. Gupta. Self-supervised exploration via disagreement. In *International conference on machine learning*, pages 5062–5071. PMLR, 2019.
- [45] A. Rahimi and B. Recht. Weighted sums of random kitchen sinks: Replacing minimization with randomization in learning. *Advances in neural information processing systems*, 21, 2008.
- [46] R. Raileanu and T. Rocktäschel. RIDE: rewarding impact-driven exploration for procedurally-generated environments. In *8th International Conference on Learning Representations*, 2020.
- [47] T. Schaul and M. Ring. Better generalization with forecasts. In *Twenty-Third International Joint Conference on Artificial Intelligence*, 2013.
- [48] T. Schaul, H. van Hasselt, J. Modayil, M. White, A. White, P.-L. Bacon, J. Harb, S. Mourad, M. Bellemare, and D. Precup. The barbados 2018 list of open issues in continual learning. *arXiv preprint arXiv:1811.07004*, 2018.
- [49] J. Schmidhuber. Making the world differentiable: On using fully recurrent self-supervised neural networks for dynamic reinforcement learning and planning in non-stationary environments. Technical Report FKI-126-90, TUM, 1990.
- [50] J. Schmidhuber. Reinforcement learning in Markovian and non-Markovian environments. In D. S. Lippman, J. E. Moody, and D. S. Touretzky, editors, *Advances in Neural Information Processing Systems 3 (NIPS 3)*, pages 500–506. Morgan Kaufmann, 1991.
- [51] J. Schmidhuber. Curious model-building control systems. In *Proceedings of the International Joint Conference on Neural Networks, Singapore*, volume 2, pages 1458–1463. IEEE press, 1991.
- [52] J. Schmidhuber. A possibility for implementing curiosity and boredom in model-building neural controllers. In *Proc. of the international conference on simulation of adaptive behavior: From animals to animats*, pages 222–227, 1991.
- [53] J. Schmidhuber. What’s interesting? Technical Report IDSIA-35-97, IDSIA, 1997. <ftp://ftp.idsia.ch/pub/juergen/interest.ps.gz>; extended abstract in Proc. Snowbird’98, Utah, 1998; see also [54].
- [54] J. Schmidhuber. Exploring the predictable. In A. Ghosh and S. Tsuitsui, editors, *Advances in Evolutionary Computing*, pages 579–612. Springer, 2002.
- [55] J. Schmidhuber. Simple algorithmic principles of discovery, subjective beauty, selective attention, curiosity & creativity. In *International conference on discovery science*, pages 26–38. Springer, 2007.
- [56] J. Schmidhuber. Formal theory of creativity, fun, and intrinsic motivation (1990–2010). *IEEE transactions on autonomous mental development*, 2(3):230–247, 2010.

- [57] J. Schulman, F. Wolski, P. Dhariwal, A. Radford, and O. Klimov. Proximal policy optimization algorithms. *arXiv preprint arXiv:1707.06347*, 2017.
- [58] R. Sekar, O. Rybkin, K. Daniilidis, P. Abbeel, D. Hafner, and D. Pathak. Planning to explore via self-supervised world models. In *International Conference on Machine Learning*, pages 8583–8592. PMLR, 2020.
- [59] P. Shyam, W. Jaśkowski, and F. Gomez. Model-based active exploration. In *International conference on machine learning*, pages 5779–5788. PMLR, 2019.
- [60] J. Storck, S. Hochreiter, J. Schmidhuber, et al. Reinforcement driven information acquisition in non-deterministic environments. In *Proceedings of the international conference on artificial neural networks, Paris*, volume 2, pages 159–164. Citeseer, 1995.
- [61] A. L. Strehl and M. L. Littman. An analysis of model-based interval estimation for markov decision processes. *Journal of Computer and System Sciences*, 74(8):1309–1331, 2008.
- [62] M. Strens. A bayesian framework for reinforcement learning. In *ICML*, volume 2000, pages 943–950, 2000.
- [63] Y. Sun, F. Gomez, and J. Schmidhuber. Planning to be surprised: Optimal bayesian exploration in dynamic environments. In *International conference on artificial general intelligence*, pages 41–51. Springer, 2011.
- [64] R. S. Sutton. Learning to predict by the methods of temporal differences. *Machine learning*, 3(1):9–44, 1988.
- [65] R. S. Sutton. Integrated architectures for learning, planning, and reacting based on approximating dynamic programming. In *Machine learning proceedings 1990*, pages 216–224. Elsevier, 1990.
- [66] R. S. Sutton and B. Tanner. Temporal-difference networks. In *Advances in neural information processing systems*, pages 1377–1384, 2005.
- [67] R. S. Sutton, J. Modayil, M. Delp, T. Degris, P. M. Pilarski, A. White, and D. Precup. Horde: a scalable real-time architecture for learning knowledge from unsupervised sensorimotor interaction. In L. Sonenberg, P. Stone, K. Tumer, and P. Yolum, editors, *10th International Conference on Autonomous Agents and Multiagent Systems (AAMAS 2011), Taipei, Taiwan, May 2-6, 2011, Volume 1-3*, pages 761–768, 2011.
- [68] R. S. Sutton, M. C. Machado, G. Z. Holland, D. S. F. Timbers, B. Tanner, and A. White. Reward-respecting subtasks for model-based reinforcement learning. *arXiv preprint arXiv:2202.03466*, 2022.
- [69] E. Talvitie. Model regularization for stable sample rollouts. In *UAI*, pages 780–789, 2014.
- [70] S. B. Thrun. Efficient exploration in reinforcement learning. 1992.
- [71] D. Ulyanov, A. Vedaldi, and V. Lempitsky. Deep image prior. In *Proceedings of the IEEE conference on computer vision and pattern recognition*, pages 9446–9454, 2018.
- [72] H. Van Seijen, M. Fatemi, and A. Tavakoli. Using a logarithmic mapping to enable lower discount factors in reinforcement learning. *Advances in Neural Information Processing Systems*, 32, 2019.
- [73] V. Veeriah, M. Hessel, Z. Xu, R. Lewis, J. Rajendran, J. Oh, H. van Hasselt, D. Silver, and S. Singh. Discovery of useful questions as auxiliary tasks. *arXiv preprint arXiv:1909.04607*, 2019.
- [74] L. Willems. Rl starter files. <https://github.com/lcswillems/rl-starter-files>, 2017.
- [75] R. J. Williams and D. Zipser. Gradient-based learning algorithms for recurrent networks and their computational complexity. *Backpropagation: Theory, architectures, and applications*, 433: 17, 1995.

- [76] D. Zha, W. Ma, L. Yuan, X. Hu, and J. Liu. Rank the episodes: A simple approach for exploration in procedurally-generated environments. *arXiv preprint arXiv:2101.08152*, 2021.
- [77] T. Zhang, H. Xu, X. Wang, Y. Wu, K. Keutzer, J. E. Gonzalez, and Y. Tian. Noveld: A simple yet effective exploration criterion. *Advances in Neural Information Processing Systems*, 34, 2021.
- [78] Z. Zheng, V. Veeriah, R. Vuorio, R. L. Lewis, and S. Singh. Learning state representations from random deep action-conditional predictions. *Advances in Neural Information Processing Systems*, 34, 2021.

Checklist

1. For all authors...
 - (a) Do the main claims made in the abstract and introduction accurately reflect the paper's contributions and scope? [Yes]
 - (b) Did you describe the limitations of your work? [Yes] See section 6.
 - (c) Did you discuss any potential negative societal impacts of your work? [Yes] See section 6.
 - (d) Have you read the ethics review guidelines and ensured that your paper conforms to them? [Yes]
2. If you are including theoretical results...
 - (a) Did you state the full set of assumptions of all theoretical results? [N/A]
 - (b) Did you include complete proofs of all theoretical results? [N/A]
3. If you ran experiments...
 - (a) Did you include the code, data, and instructions needed to reproduce the main experimental results (either in the supplemental material or as a URL)? [Yes] Included in the supplementary material. An open-source implementation will be made available online.
 - (b) Did you specify all the training details (e.g., data splits, hyperparameters, how they were chosen)? [Yes] Implementation details and hyperparameters are provided in Appendices B and C
 - (c) Did you report error bars (e.g., with respect to the random seed after running experiments multiple times)? [Yes] We include 95% bootstrapped confidence intervals over 5 or 10 seeds for all of our results.
 - (d) Did you include the total amount of compute and the type of resources used (e.g., type of GPUs, internal cluster, or cloud provider)? [Yes] Details provided in Appendix C
4. If you are using existing assets (e.g., code, data, models) or curating/releasing new assets...
 - (a) If your work uses existing assets, did you cite the creators? [Yes]
 - (b) Did you mention the license of the assets? [Yes] Provided in Appendix A.2 with the description of the environment.
 - (c) Did you include any new assets either in the supplemental material or as a URL? [N/A]
 - (d) Did you discuss whether and how consent was obtained from people whose data you're using/curating? [N/A]
 - (e) Did you discuss whether the data you are using/curating contains personally identifiable information or offensive content? [N/A]
5. If you used crowdsourcing or conducted research with human subjects...
 - (a) Did you include the full text of instructions given to participants and screenshots, if applicable? [N/A]
 - (b) Did you describe any potential participant risks, with links to Institutional Review Board (IRB) approvals, if applicable? [N/A]
 - (c) Did you include the estimated hourly wage paid to participants and the total amount spent on participant compensation? [N/A]

A Environments

In the following sections we describe the environments used in our experiments.

A.1 Diabolical lock

The diabolical lock problem [36] consists of states organised in 3 rows $\{a, b, c\}$ and H columns from $\{1, 2, \dots H\}$ (see Figure 6). In each episode, the agent is initialised in one of two possible starting states, either at a_1 or b_1 with equal probability. Each episode lasts for H time steps.

Transition dynamics In each state the agent has L available actions, only one of which is ‘good’ and transitions to a ‘good’ state (green) in the next column with equal probability. For instance, the good action in state a_t leads to a_{t+1} or b_{t+1} with equal probability. Taking the good action gives a negative (anti-shaped) reward of $-1/H$, except at the end of the lock (states a_H or b_H), where the sparse optimal reward of 10 is received. The remaining $L - 1$ actions in any state are ‘bad,’ causing a deterministic transition to the ‘dead’ row c (red) at the next column (with zero reward). The agent remains in the ‘dead’ row c till the end of the episode, i.e., all actions from c_t transition to c_{t+1} with zero reward. The good action in each state is assigned uniformly at random from the L available actions upon initialising the environment. The good action in every state remains fixed across episodes.

Noisy observations The diabolical lock environment provides a high-dimensional noisy observation based on the environmental state. The observation is obtained by concatenating one-hot vectors encoding the row and column, adding independent Gaussian noise with variance σ_o^2 to each component of the vector, padding this vector with zeroes to the nearest higher power of two and then applying a Hadamard rotation matrix.

In our experiments, we select $H = 100$, $L = 10$, and $\sigma_o = 0.1$, which is similar to the configuration used by Misra et al. [36]. We were unable to find a publicly available implementation of the environment introduced by Misra et al. [36] and therefore used our own (no license).

A.2 MiniGrid

The MiniGrid [13] (Apache License 2.0) set of environments are partially observable, procedurally generated, and provide a sparse reward upon successful completion of the task.

The agent receives a 7×7 egocentric view of its surroundings, which is a $7 \times 7 \times 3$ integer encoding that describes the contents of the visible grid cells. The agent cannot see behind walls or closed doors.

For the study with *panoramic observations*, we follow the implementation of Parisi et al. [42] where a rotation invariant view is created by concatenating the four observations from when the agent faces north, east, south and west to create a $7 \times 7 \times 12$ panoramic observation.

At every step, the agent has seven available actions: turn left, turn right, move forward, pick up, drop, toggle (used to open doors), and done.

A new configuration of the environment is generated for each episode. Episodes finish when the agent has interacted with the environment for the maximum number of steps permitted, or if the agent successfully completes the task, in which case it also receives a non-zero reward depending on the number of steps taken to complete the task.

KeyCorridor The agent has to pick up a ball behind a locked door. To unlock the door, the agent must first find the key, which is also hidden behind closed (but unlocked) doors. We consider two levels of difficulty in this class of environments. The KeyCorridor-S5R3 environment poses a harder exploratory challenge due to larger rooms and hallways in comparison to KeyCorridor-S4R3.

ObstructedMaze Like with the KeyCorridor environments, the goal of the agent is to pick up a ball behind one of the locked doors. We again consider two levels of difficulty in this class of environments. In the ObstructedMaze-2Dlh environment the keys are hidden inside chests. In ObstructedMaze-2Dlhb the keys are hidden inside chests and the doors are blocked by obstacles that need to be displaced.

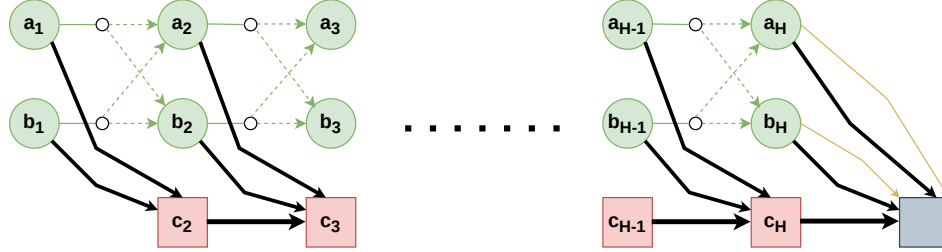


Figure 6: Based on Figure 5 from Misra et al. [36]. The diabolical lock environment is organised in 3 rows $\{a, b, c\}$ and H columns. The green states of rows a and b correspond to the ‘good’ states. The red states of row c correspond to the ‘dead’ states. The grey square denotes the terminal state. The black arrows represent deterministic transitions to the ‘dead’ row of the next column. The green dotted arrows denote the equally likely transitions to one of two good states by taking the ‘good’ action. The yellow arrows mark the final transitions which provide the optimal sparse reward upon termination.

MultiRoom The goal of the agent is to reach the goal state in the farthest room. The notation N12-S10 signifies that the environment consists of 12 rooms with a maximum size of 10. These environments (MultiRoom-N7-S8 and MultiRoom-N12-S10) are not available in the default set of MiniGrid environments. We borrow the implementation of these environments from previous work [46](Creative Commons Attribution-NonCommercial 4.0 International Public License).

B Implementation details for diabolical lock experiments

This section presents the implementation details for our experiments with the diabolical lock environment. In the following, we describe the architectures and hyperparameters of our actor, critic, pseudo-reward generator, and ensemble of predictors used in these experiments.

B.1 Neural network architectures

Base agent We use the PPO [57] implementation from the `rl-starter-files` repository [74]. The actor and critic share a multi-layer perceptron (MLP) of three layers with 256 units and ReLU non-linearities. Separate linear heads for the actor and critic operate on the representation provided by the shared architecture.

Pseudo-reward generator The randomly initialised fixed network for generating pseudo-rewards is a two layer MLP with ReLU non-linearities in the hidden layer of 128 units. The linear output layer provides a vector of 128 pseudo-rewards.

Predictor networks The predictor network for RND has the same architecture as the pseudo-reward generator.

The predictor network for RC-GVF is an MLP (no recurrence here) with wider layers and one extra layer compared to the pseudo-reward generating network. Specifically, a predictor consists of a network of three layers with 256 units each with ReLU non-linearities in the two hidden layers. We use an ensemble of $K = 2$ predictors in the case of RC-GVF. In these experiments with the diabolical lock, the individual predictors in the ensemble are completely separate neural networks which do not share parameters.

B.2 Grid search and hyperparameters

Hyperparameters of the base PPO agent are provided in Table 2. These were selected based on previous work [36] and apply to our method and RND.

Utilising an intrinsic reward introduces additional hyperparameters. We conducted a grid-search to select the values for hyperparameters introduced by RND and RC-GVF. The best hyperparameter configuration was selected by evaluating average lock completion for each candidate in the grid

Table 2: PPO hyperparameters for diabolical lock experiments.

Hyperparameter	Value
Discount factor	0.99
GAE lambda	0.95
Optimization epochs	5
Learning rate (η)	0.0005
Clipping epsilon	0.2
Rollout length (frames per process) $H = 100$	
Batch size	256
Parallel processes	16
Entropy coefficient	0.01
Value loss coefficient	0.5

across 5 seeds. In Table 1, we report the final results with 10 independent runs of the selected hyperparameters.

For RND, the hyperparameters include the intrinsic coefficient β and the learning rate of the predictor η_p . The search candidates and the final selected values are described in Table 3.

Table 3: RND specific hyperparameters for diabolical lock experiments.

Hyperparameter	Candidates	Selected
Predictor learning rate η_p	$\{\eta, 0.75\eta, 0.5\eta, 0.25\eta, 0.1\eta\}$	0.25η ($\eta = 0.0005$)
Intrinsic reward coefficient β	$\{4.0, 2.0, 1.0, 0.5, 0.25\}$	0.5

In comparison to RND, RC-GVF introduces additional hyperparameters such as the GVF discount factor γ_z , the associated bias-variance tradeoff parameter for the TD-targets λ_z , and the number of predictors in the ensemble. We observed good results with our default values of $\gamma_z = 0.6$ and an ensemble of 2 predictors. The search candidates and the final selected values for RC-GVF are described in Table 4.

Table 4: RC-GVF specific hyperparameters for diabolical lock experiments.

Hyperparameter	Candidates	Selected
Number of predictors	$\{2\}$	2
Predictor learning rate η_p	$\{\eta, 0.5\eta, 0.25\eta\}$	0.5η ($\eta = 0.0005$)
Intrinsic reward coefficient β	$\{4.0, 2.0, 1.0, 0.5\}$	2.0
GVF discount factor γ_z	$\{0.6\}$	0.6

The learning rates of the base agent and predictor are linearly annealed to zero over 100 million frames. We used the Adam optimiser [29] for the PPO agent and the predictor in all experiments.

C Implementation details for Minigrid experiments

This section presents the implementation details for our experiments with the MiniGrid environments.

C.1 Neural network architectures

Base agent We use the PPO implementation from the `rl-starter-files` [74] repository. We retain the same architecture for the actor and critic as provided in their implementation.

The actor and the critic share three convolution layers with 16, 32 and 64 output channels, with 2×2 kernels and a stride of 1. Each convolution layer is followed by a ReLU non-linearity. A 2×2 max-pooling is applied after the first convolution layer. The output from the convolution layers is flattened and provided to an LSTM [21] with a hidden dimension of 64. Separate multi-layer perceptron (MLP) heads for the actor and critic operate on the output of the LSTM to output the

action logits and the value. Each MLP has 64 hidden units with a hyperbolic tangent (tanh) activation function.

Pseudo-reward generator The pseudo-reward generator is implemented as a convolutional neural network whose output is flattened to provide a vector of pseudo-rewards $z_{t+1} \in \mathbb{R}^d$. It has a similar architecture to the convolutional layers used in the base agent.

Concretely, this network consists of three convolution layers, with 32, 64, and d output channels respectively, with 2×2 kernels and a stride of 1. Here, d is the number of pseudo-rewards, which we set as $d = 128$ for our experiments. ReLU non-linearity is applied after the first two convolution layers. Additionally, a 2×2 max-pooling is applied after the first convolution layer.

Predictor networks In the case of RND, the predictor network has the same architecture as the pseudo-reward generator.

For RC-GVF, we have an ensemble of predictors with K members. An ensemble of K two layer MLP heads (with 256 units and ReLU non-linearity) operate on a common representation of 128 dimensions generated by a shared recurrent (LSTM) core. The LSTM operates on histories of observations, actions, and pseudo-rewards.

The observation at time step o_t is fed through three convolution layers with 32, 64 and 128 output channels, with 2×2 kernels and a stride of 1. Each convolution layer is followed by a ReLU non-linearity. A 2×2 max-pooling is applied after the first convolution layer. The output from the convolution layers is flattened and provided to a fully connected layer which provides a 64 dimensional representation of the input observation.

The action at the previous time step a_{t-1} (as a one-hot input) is transformed into a 32 dimensional vector by a fully connected layer. A fully connected layer is also applied to the previous pseudo-reward vector z_t to obtain a 32 dimensional vector. The observation, action and pseudo-reward representations are concatenated into a 128 dimensional vector which is fed as input to the LSTM (with hidden dimension of 128).

C.2 Details about baseline implementations

We employed the same base PPO agent (see Appendix C.1) for all approaches to maintain consistency. This means that our implementation of baselines deviate slightly from the original implementations. Nevertheless, we obtain comparable or better results than the reported ones on the considered environments. We describe the key details of our AGAC [18] and NovelD [77] implementations below.

AGAC The PPO implementation of AGAC utilised independent convolutional neural networks for the actor and critic with frame stacking rather than a shared recurrent neural network (for actor and critic) as used by us.

In our implementation, the policy predictor (or adversary) has the same architecture as the recurrent actor-critic (see Appendix C.1), but without the MLP head for the critic.

NovelD NovelD derives intrinsic rewards using RND as a novelty measure. The neural network architecture details for NovelD therefore follow those described for RND (see Appendix C.1).

A major difference is that the original implementation of NovelD used IMPALA [16] as the base agent instead of PPO.

Another deviation in our version of NovelD is that we do not use the *Episodic Restriction on Intrinsic Reward (ERIR)* multiplier for using episodic counts. The ERIR multiplier uses episodic counts from the simulator to ensure that intrinsic rewards are provided only when the agent visits a state for the first time in an episode. For consistency, we use episodic counts in a similar manner to RIDE [46] and AGAC [18], where the square root of episodic count divides the main intrinsic reward term. Our

NovelD intrinsic reward is given by⁴

$$R_i(o_t; s_t, o_{t+1}) = \frac{\max[\text{novelty}(o_{t+1}) - \alpha \cdot \text{novelty}(o_t), 0]}{\sqrt{N_e(s_t)}}, \quad (9)$$

where $\text{novelty}(\cdot)$ is measured as the RND prediction error (see Equation 2), α is a hyperparameter called the scaling factor, and $N_e(s_t)$ is the number of times the agent has been in that state in that episode.

On the use of episodic counts Note that in our experiments the episodic counts refer to agent positions alone, following AGAC [18]. Other approaches have used different strategies to obtain episodic counts from the simulator. For example, RIDE [46] and NovelD [77] derive counts from fully observable views which provide count information based on agent position, direction or whether an object has been picked up etc.

C.3 Grid search and selected hyperparameters

In this section we describe our hyperparameter selection strategy for the MiniGrid experiments.

Our implementation utilises the PPO implementation from the `r1-starter-files` [74] repository. The hyperparameters for the common PPO base agent were selected via preliminary experiments and are similar to the ones provided in the `r1-starter-files` repository. These are detailed in Table 5.

Table 5: PPO hyperparameters for MiniGrid experiments.

Hyperparameter	Value
Discount factor	0.99
GAE lambda	0.95
Optimization epochs	4
Learning rate (η)	0.0002
Clipping epsilon	0.2
Rollout length (frames per process)	128
Batch size	256
Parallel processes	16
Value loss coefficient	0.5
Recurrence (for truncated BPTT [75])	4

We choose the hyperparameters introduced by each intrinsic reward approach via a grid search. We select separate hyperparameters for each environment type: MultiRoom, KeyCorridor and ObstructedMaze. To select hyperparameters, we evaluate each candidate configuration with 5 seeds on the simpler versions of the considered environments (MultiRoom-N7S8, KeyCorridor-S4R3 and ObstructedMaze-2Dlh) and select the configuration with the highest average return.

Final results are reported with separate independent runs on these environments (usually with 10 seeds) and also the harder versions of the considered environments (MultiRoom-N12S10, KeyCorridor-S5R3 and ObstructedMaze-2Dlhb).

All experiments used the Adam optimiser [29] for the PPO agent and the respective predictors.

Similar to previous approaches [46, 18], the learning rates are linearly annealed to zero while interacting with the environment during 10 million frames for the MultiRoom environments, 30 million frames for the KeyCorridor and ObstructedMaze-2Dlh environments, and 90 million frames for the ObstructedMaze-2Dlhb environment.

C.3.1 RC-GVF

We selected the GVF discount factor $\gamma_z = 0.6$ and the associated λ -return parameter $\lambda_z = 0.9$ as default values for all experiments. We found that $K = 2$ predictors in the ensemble worked

⁴We note that the authors of NovelD mention that replacing the ERIR term with scaling based on the square root of episodic counts still outperforms previous baselines (<https://openreview.net/forum?id=CyUzpn0kFJp>).

sufficiently well in preliminary experiments. We identified the entropy coefficient, intrinsic reward coefficient and learning rate of the predictor through a grid search. The candidate and selected values are described in Tables 6 and 7 for the setting with egocentric and panoramic observations respectively.

Table 6: RC-GVF specific hyperparameters for MiniGrid experiments with egocentric observations.

Hyperparameter	Candidates	Egocentric observations		
		MultiRoom	KeyCorridor	ObstructedMaze
Number of predictors	{2}	2	2	2
GVF discount factor γ_z	{0.6}	0.6	0.6	0.6
GVF λ_z (for TD- λ targets)	{0.9}	0.9	0.9	0.9
Predictor learning rate η_p	{0.5 η , 0.75 η , η }	0.75 η	0.75 η	0.75 η
Intrinsic reward coefficient β	{0.1, 0.5, 1.0}	1.0	0.1	0.1
Entropy coefficient	{0, 1e-5, 1e-4, 1e-3}	1e-5	1e-5	1e-4

Table 7: RC-GVF specific hyperparameters for MiniGrid experiments with panoramic observations.

Hyperparameter	Candidates	Panoramic observations		
		MultiRoom	KeyCorridor	ObstructedMaze
Number of predictors	{2}	2	2	2
GVF discount factor γ_z	{0.6}	0.6	0.6	0.6
GVF λ_z (for TD- λ targets)	{0.9}	0.9	0.9	0.9
Predictor learning rate η_p	{0.5 η , 0.75 η , η }	0.5 η	0.75 η	0.5 η
Intrinsic reward coefficient β	{0.1, 0.5, 1.0}	0.1	1.0	0.1
Entropy coefficient	{0, 1e-5, 1e-4, 1e-3}	1e-5	1e-5	1e-4

C.3.2 RND

Tables 8 and 9 describe the search grid and selected hyperparameters for RND with egocentric and panoramic observations respectively.

Table 8: RND specific hyperparameters for MiniGrid experiments with egocentric observations.

Hyperparameter	Candidates	Egocentric observations		
		MultiRoom	KeyCorridor	ObstructedMaze
Predictor learning rate η_p	{0.5 η , 0.75 η , η }	0.75 η	0.75 η	0.75 η
Intrinsic reward coefficient β	{0.0001, 0.0005, 0.001, 0.005}	0.0005	0.0005	0.0005
Entropy coefficient	{0, 1e-5, 1e-4, 1e-3}	0	1e-5	1e-4

Table 9: RND specific hyperparameters for MiniGrid experiments with panoramic observations.

Hyperparameter	Candidates	Panoramic observations		
		MultiRoom	KeyCorridor	ObstructedMaze
Predictor learning rate η_p	{0.5 η , 0.75 η , η }	0.75 η	0.75 η	0.75 η
Intrinsic reward coefficient β	{0.0001, 0.0005, 0.001, 0.005}	0.0005	0.001	0.0001
Entropy coefficient	{0, 1e-5, 1e-4, 1e-3}	1e-5	1e-5	1e-4

C.3.3 NovelD

NovelD relies on RND as a novelty measure and therefore has similar hyperparameters. We identified the entropy coefficient, intrinsic coefficient and learning rate of the RND predictor through a grid search.

A new hyperparameter introduced by NovelD is the scaling factor (α in Equation 9) which was selected as 0.5 in previous work [77]. We also found the value of 0.5 to work well in our preliminary experiments and did not search over other values for this hyperparameter.

Tables 10 and 11 describe the search grid and selected hyperparameters for NovelD.

Table 10: NovelD specific hyperparameters for MiniGrid experiments with egocentric observations (without counts).

Hyperparameter	Candidates	Without episodic counts		
		MultiRoom	KeyCorridor	ObstructedMaze
Scaling factor α	{0.5}	0.5	0.5	0.5
Predictor learning rate η_p	{0.5 η , 0.75 η , η }	0.5 η	0.75 η	0.75 η
Intrinsic reward coefficient	{0.0005, 0.001, 0.005, 0.01}	0.01	0.005	0.001
Entropy coefficient	{0, 1e-5, 1e-4, 1e-3}	0	1e-5	1e-4

Table 11: NovelD specific hyperparameters for MiniGrid experiments with episodic counts.

Hyperparameter	Candidates	With episodic counts		
		MultiRoom	KeyCorridor	ObstructedMaze
Scaling factor α	{0.5}	0.5	0.5	0.5
Predictor learning rate η_p	{0.5 η , 0.75 η , η }	0.75 η	0.75 η	0.75 η
Intrinsic reward coefficient β	{0.005, 0.01, 0.05, 0.1}	0.05	0.01	0.01
Entropy coefficient	{0, 1e-5, 1e-4, 1e-3}	1e-5	1e-5	1e-4

C.3.4 AGAC

We identified the entropy coefficient, intrinsic coefficient and learning rate of the predictor (‘adversary’ in the original terminology) through a grid search.

AGAC also introduces a hyperparameter called the ‘episodic count coefficient’ to scale the bonus from the episodic counts term.

Our main results in Figure 2 are obtained without the use of episodic counts (this coefficient is set to zero). To report results with episodic counts in Figure 3 we search over values of this hyperparameter.

Tables 12 and 13 describe the search grid and selected hyperparameters for AGAC.

Note that in the experiments without episodic counts, AGAC did not succeed (with any search configuration) on any environment other than ObstructedMaze-2Dlh.

Table 12: AGAC specific hyperparameters for MiniGrid experiments with egocentric observations (without counts).

Hyperparameter	Candidates	Without episodic counts		
		MultiRoom	KeyCorridor	ObstructedMaze
Predictor learning rate η_p	{0.25 η , 0.5 η }	0.25 η	0.25 η	0.25 η
Intrinsic coefficient	{0.00001, 0.00005, 0.0001, 0.0005}	0.00005	0.00005	0.00005
Episodic count coefficient	{0}	0	0	0
Entropy coefficient	{0, 1e-5, 1e-4, 1e-3}	1e-5	1e-4	1e-4

C.4 Grid search and selected hyperparameters for analysis and ablation

For the analysis of discount factors presented in Figures 4a and 4b we conducted a search over best intrinsic reward coefficients (β) for each GVF discount factor γ_z . This was necessary as the magnitudes of the TD-error are sensitive to the choice of γ_z . The candidates and selected intrinsic reward coefficients (β) are reported in Table 14. The remaining hyperparameters are the same as the

Table 13: AGAC specific hyperparameters for MiniGrid experiments with episodic counts

Hyperparameter	Candidates	With episodic counts		
		MultiRoom	KeyCorridor	ObstructedMaze
Predictor learning rate η_p	$\{0.25\eta, 0.5\eta\}$	0.25η	0.25η	0.25η
Intrinsic coefficient	$\{0.00001, 0.00005, 0.0001, 0.0005\}$	0.00005	0.00005	0.00005
Episodic count coefficient	$\{0.0005, 0.001, 0.005, 0.01\}$	0.005,	0.001	0.001
Entropy coefficient	$\{0, 1e-5, 1e-4, 1e-3\}$	$1e-5$	$1e-4$	$1e-4$

ones selected for RC-GVF with panoramic views (see Table 7). Final results are reported with 10 independent runs of the selected hyperparameters.

Table 14: Search over intrinsic coefficients for different GVF discount factors. KCS5R3 refers to the KeyCorridor-S5R3 environment and MRN12S10 refers to the MultiRoom-N12-S10 environment.

GVF γ_z	Intrinsic coefficients (β) considered	Selected β (KCS5R3)	Selected β (MRN12S10)
0.99	$\{1e-6, 5e-6, 1e-5, 5e-5, 1e-4, 5e-4, 1e-3, 5e-3\}$	$1e-5$	$1e-4$
0.95	$\{0.0005, 0.001, 0.005, 0.01, 0.05\}$	0.001	0.001
0.7	$\{0.1, 0.5, 1\}$	0.5	0.1
0.6	$\{0.1, 0.5, 1\}$	1	0.1
0.3	$\{0.5, 1, 5, 10, 25, 50\}$	10	1
0.1	$\{1, 5, 10, 25, 50, 100\}$	25	5
0.05	$\{1, 5, 10, 25, 50, 100\}$	25	10
0.0	$\{5, 10, 25, 50, 100\}$	50	10

We conduct a similar search over choices of intrinsic coefficients for the ablation with components of RC-GVF (see Figure 5). The candidates and selected intrinsic reward coefficients are reported in Table 15. The hyperparameters for RC-GVF ($\gamma_z = 0.6$) and RND are the same as the ones reported in Tables 7 and 9 respectively. Final results are reported with 10 independent runs of the selected hyperparameters.

Table 15: Search over intrinsic coefficients for different variants of RC-GVF. KCS5R3 refers to the KeyCorridor-S5R3 environment.

Approach	Intrinsic coefficients (β) considered	Selected β (KCS5R3)
RC-GVF ($\gamma_z = 0.0$)	$\{5, 10, 25, 50, 100\}$	50
RC-GVF ($\gamma_z = 0.0$) w/o disagreement	$\{0.0005, 0.001, 0.005, 0.01\}$	0.005
RC-GVF ($\gamma_z = 0.0$) w/o recurrence	$\{10, 25, 50, 100\}$	50
RC-GVF ($\gamma_z = 0.6$) w/o disagreement	$\{0.00001, 0.00005, 0.0001, 0.0005\}$	0.00005
RC-GVF ($\gamma_z = 0.6$) w/o recurrence	$\{0.1, 0.5, 1\}$	0.5

C.5 Computational resources

All our experiments were conducted on a cluster with NVIDIA Pascal P100 GPUs. Due to low GPU usage of a single run, we could accommodate multiple concurrent runs (usually 5) on the same node (CPU + GPU). Our final experiments should be easy to replicate even on a single GPU machine. A single run of RC-GVF on a desktop machine with an NVIDIA GeForce RTX 2080 GPU completes about 30 million frames in MiniGrid (with egocentric observations) in about 9 hours (equivalent to our KeyCorridor experiments).

D Additional experiments with the diabolical lock problem

D.1 Further baselines

Our aim with the diabolical lock experiment is to illustrate the differences between RND and RC-GVF. For completeness, in this section, we additionally report the performance of AGAC and NovelD. We

also investigate the performance of RND with a higher capacity predictor, as used by RC-GVF (see Appendix B).

We conduct a grid-search to select the values for hyperparameters specific to the new baselines. These are described in Tables 17, 18, and 19. The best configuration is selected by evaluating average lock completion for each candidate in the grid across 5 seeds. The remaining hyperparameters are the same as the ones detailed in Appendix B.2.

The farthest completions at different points in training (with 10 independent runs of the selected hyperparameters) are reported in Table 20. We observe that neither AGAC nor NovelD manage to complete the lock. AGAC does not make much progress towards solving the problem. NovelD fares better and performs roughly as well as RND. We also observe that the higher capacity predictor does not improve RND (on average).

Table 16: Mean over 10 seeds and (min, max) of the farthest column reached (of $H = 100$) at different points on the diabolical lock problem.

Frames	5M	10M	15M	20M
RC-GVF	61 (47, 81)	94 (83, 100)	100 (100, 100)	100 (100, 100)
RND	28 (21, 41)	37 (27, 47)	41 (30, 53)	46 (33, 58)
RND (with high capacity predictor)	22 (8, 41)	28 (8, 62)	32 (8, 70)	34 (8, 72)
NovelD	28 (22, 35)	35 (26, 50)	41 (27, 54)	45 (32, 60)
AGAC	5 (5, 7)	6 (5, 7)	6 (5, 9)	6 (5, 9)

Table 17: RND (with high capacity predictor) hyperparameters for diabolical lock experiments.

Hyperparameter	Candidates	Selected
Predictor learning rate η_p	$\{\eta, 0.75\eta, 0.5\eta, 0.25\eta\}$	0.25η ($\eta = 0.0005$)
Intrinsic reward coefficient β	$\{4.0, 2.0, 1.0, 0.5, 0.25\}$	1.0

Table 18: NovelD specific hyperparameters for diabolical lock experiments.

Hyperparameter	Candidates	Selected
Predictor learning rate η_p	$\{\eta, 0.75\eta, 0.5\eta, 0.25\eta\}$	0.25η ($\eta = 0.0005$)
Intrinsic reward coefficient β	$\{4.0, 2.0, 1.0, 0.5, 0.25\}$	1.0
Scaling factor α	$\{0.5\}$	0.5

Table 19: AGAC specific hyperparameters for diabolical lock experiments.

Hyperparameter	Candidates	Selected
Predictor learning rate η_p	$\{0.5\eta, 0.25\eta\}$	0.25η ($\eta = 0.0005$)
Intrinsic reward coefficient β	$\{4.0, 2.0, 1.0, 0.5, 0.25\}$	1.0
Shared architecture for actor and critic	$\{True, False\}$	<i>True</i>

D.2 Ensemble size analysis

In this section, we analyse the effect of increasing the ensemble size in RC-GVF on the performance in the diabolical lock problem. We consider 2, 4, 6 and 8 predictors in the ensemble. The other hyperparameters are the same as those reported in Table 4.

The results are reported across 10 seeds in Table 20. For the most part, we obtain similar results for the different ensemble sizes. The minor exception is with 6 predictors, where one run out of the ten fails to reach the end of the lock.

Table 20: Mean over 10 seeds and (min, max) of the farthest column reached (of $H = 100$) at different points during training on the diabolical lock problem. Higher is better.

Number of predictors / Frame	5M	10M	15M	20M
2	61 (47, 81)	94 (83, 100)	100 (100, 100)	100 (100, 100)
4	66 (62, 78)	96 (82, 100)	100 (100, 100)	100 (100, 100)
6	61 (39, 75)	90 (59, 100)	96 (63, 100)	97 (67, 100)
8	69 (57, 84)	94 (77, 100)	100 (99, 100)	100 (100, 100)

E Additional experiments in MiniGrid

E.1 Intrinsic reward from solely episodic counts

Figure 7 shows that intrinsic rewards from episodic state counts are sufficient for solving the MultiRoom-N7S8 and MultiRoom-N12S10 environments.

The exact form of the intrinsic bonus is $R_i(s_t) = \frac{\beta}{\sqrt{N_e(s_t)}}$, where $N_e(s_t)$ is the number of times the agent has been in that position in that episode, and β is the intrinsic reward coefficient.

We perform a search over the intrinsic reward coefficients $\beta \in \{0.0005, 0.001, 0.005, 0.01\}$ and select $\beta = 0.005$ as a suitable value. The entropy coefficient for this experiment is set to 0.00001.

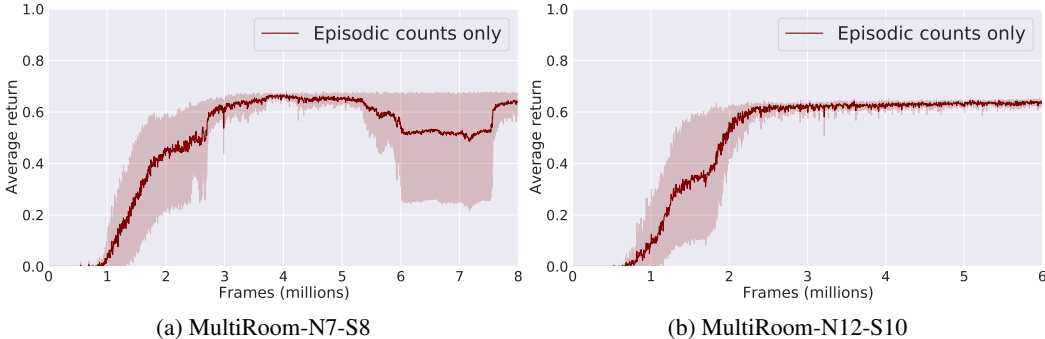


Figure 7: Performance with an intrinsic reward derived from episodic counts. These results show that a bonus term from solely episodic counts can guide useful exploration in MiniGrid environments. 95% bootstrapped confidence intervals are shown for 5 seeds.

E.2 RC-GVF with episodic counts

Several recent works incorporate episodic counts from the simulator as part of their intrinsic reward in MiniGrid [46, 18, 77]. Our main experiments with RC-GVF do not utilise episodic counts as we do not wish to provide agents with access to privileged information. For completeness, this section reports the result from a preliminary experiment, where we study the performance of RC-GVF with the use of episodic counts. We incorporate episodic counts in the same way as for the other baselines (see Appendix C.2).

To account for change in scale of the intrinsic reward with the use of the counts, we perform a search over the intrinsic reward coefficients $\beta \in \{1, 5, 10\}$ and select $\beta = 5$ for KeyCorridor-S5R3 and $\beta = 1$ for MultiRoom-N12-S10. All other hyperparameters are the same as those reported in Table 6.

As shown in Figure 8, RC-GVF can solve the harder environments (KeyCorridor-S5R3 and MultiRoom-N12-S10) without panoramic observations when including episodic counts. In KeyCorridor-S5R3 we observe that RC-GVF adapted in this way is competitive with the baselines, while in MultiRoom-N12-S10 it converges more slowly. This is unsurprising since we have not attempted to make our approach amenable to incorporating episodic counts. Indeed, in MultiRoom-N12-S10, we observe that RC-GVF performs worse compared to when only using episodic state-counts (and no value function prediction), indicating that some interference takes place between these two signals. Thus, we expect that other ways of combining (or weighting) these signals (such

as by using an additive term for the state-counts as opposed to a multiplicative one) should lead to improved performance when also including state-counts.

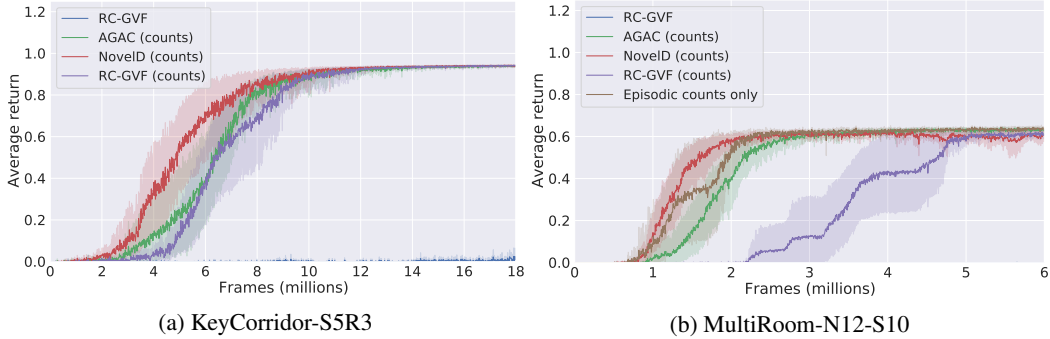


Figure 8: These results show that the performance of RC-GVF can also be improved through the use of episodic counts. All approaches use the standard egocentric observations. 95% bootstrapped confidence intervals are shown for 10 seeds.

E.3 Improvement from history conditioning

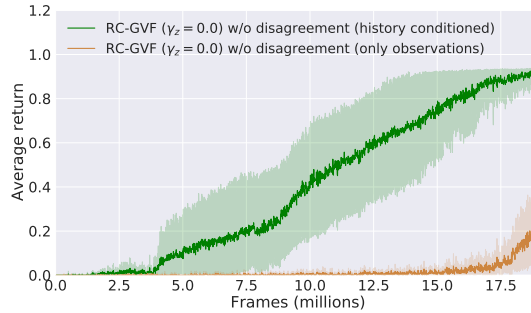


Figure 9: Studying the performance of RC-GVF ($\gamma_z = 0$) without the disagreement term on the KeyCorridor-S5R3 environment. We see that our recurrent predictor conditioned on histories of observations, actions and pseudo-rewards performs better than one conditioned on just histories of observations. 95% bootstrapped confidence intervals are shown for 10 seeds.

As indicated in Figure 5a, the recurrent predictor plays an important role in the functioning of RC-GVF. Here we present a result which shows that a recurrent predictor conditioned on histories of observations, actions and pseudo-rewards outperforms a recurrent predictor operating on histories of observations. Figure 9 compares the performance of the two variants on the KeyCorridor-S5R3 environment. We hypothesise that the improved results with history conditioning arise from previous pseudo-rewards being made available to the predictor. In a procedurally generated environment, having access to previous pseudo-rewards could support predictions of the new input observations on which the predictor has not yet been trained.

E.4 Ensemble size analysis

Figure 10 shows the performance of larger ensemble sizes with RC-GVF in two MiniGrid environments (KeyCorridor-S5R3 and MultiRoom-N12-S10). We observe similar results for ensemble sizes of 2, 4, 6 and 8 predictors. The intrinsic coefficient $\beta = 1$ in KeyCorridor-S5R3 and $\beta = 0.5$ in MultiRoom-N12-S10. The remaining hyperparameters are the same as the ones in Table 7.

These results indicate that two member ensembles usually suffice in these problems. We speculate how measuring disagreement with an ensemble of two predictors might be sufficient when also including the prediction error term. However, note that the ensemble members have a common recurrent core and only differ in MLP heads; perhaps having separate RNNs for each member would lead to greater variation with ensemble size.

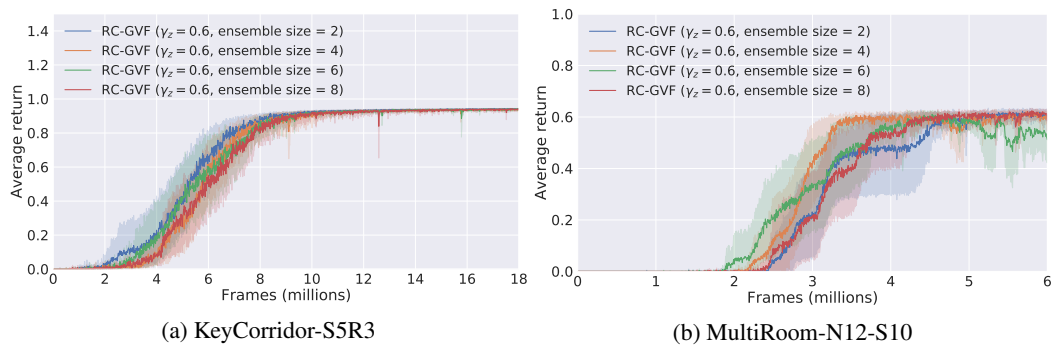


Figure 10: Comparison of RC-GVF with different numbers of predictors in the ensemble. 95% bootstrapped confidence intervals are shown for 10 seeds.